NANO · MICRO small
www.small-journal.com

Self-Healing Porous Microneedles Fabricated Via Cryogenic Micromoulding and Phase Separation for Efficient Loading and Sustained Delivery of Diverse Therapeutics

*Zhixin Ling, Yanting Zheng, Zhiming Li, Puxuan Zhao, and Hao Chang**

Sustained-release drug delivery formulations are preferable for treating various diseases as they enhance and prolong efficacy, minimize adverse effects, and avoid frequent dosing. However, these formulations are associated with poor patient compliance, require trained personnel for administration, and involve harsh manufacturing conditions that compromise drug stability. Here, a self-healing biodegradable porous microneedle (PMN) patch is reported for sustained drug delivery. The PMN patch is fabricated by a cryogenic micromoulding followed by phase separation, leading to formation of interconnected pores on the surface and internals of MNs. The pores with self-healing feature enable the PMNs to load hydrophilic drugs with different molecular weights in a mild and efficient manner. The healed PMNs can easily penetrate into the skin under press and detach from the supporting substrate under shear, thereby acting as implantable drug reservoirs for achieving sustained release of drugs for at least 40 days. One-time administration of desired therapeutics using the sustained-release healed PMNs resulted in stronger and longer-lasting efficacy in mitigating psoriasis and eliciting immunity compared to conventional methods with multiple administrations. The self-healing PMN patch for self-administrated and long-acting drug delivery can eventually improve medication adherence in prophylactic and therapeutic protocols that typically require frequent dosages.

1. Introduction

Delivery of drug molecules (also referred to as active pharmaceutical ingredients) in a sustained-release manner is highly attractive in many biomedical applications. For instance, in the treatment of chronic diseases (e. g. autoimmune skin disease, cardiovascular disease, and cancer), sustained-release drug delivery formulations can increase drug effectiveness and reduce the potential side effect by maintaining drug in the body at optimal therapeutic level, and improve patient compliance and adherence by decreasing administration frequency, compared to immediate-release drug delivery formulations.[1] Furthermore, sustained delivery of vaccines has been demonstrated to induce potent and robust adaptive immune responses by mimicking natural infection and prolonging the presentation of antigens.[2] Currently, various sustained-release delivery systems or formulations have been developed including implantable devices, polymeric micro/nanoparticles and hydrogels.[3] Unfortunately, these formulations have to rely on the hypodermic needle for administration or surgical implantation within the body. These invasive procedures are painful and cause stress, necessitate trained professionals, thereby limiting them to use in hospitals or clinics, and pose serious safety issues due to the possible re-use and injuries from sharp tools such as needles and scalpels.[4] Therefore, development of a sustained release delivery system that is painless, minimally invasive and allows self-administration is necessary in order to meet the tremendous clinic needs.

Microneedles (MNs) are regarded as an attractive drug delivery system that can pierce the stratum corneum of the skin and administer therapeutic molecules into the viable epidermis and dermis layers in a painless, efficient, and minimally invasive manner.[5] Drugs can be directly encapsulated into the matrix of MNs to form MN-based drug-device combination systems, making MNs easy to use and allowing for patient self-administration with minimal training.[6] Transdermal delivery with MNs has been extensively used for the treatment of local skin disorders and systemic diseases, as well as vaccination.[7] Currently, several types of MNs with sustained release properties have been developed, mainly including hydrogel MNs, biodegradable MNs, and MNs combined with nano/microparticles.[8] However, the fabrication of hydrogel MNs and biodegradable MNs generally

Z. Ling, Y. Zheng, Z. Li, P. Zhao, H. Chang
Hangzhou Institute of Medicine
Chinese Academy of Sciences
Hangzhou, Zhejiang 310022, China
E-mail: changhao@ibmc.ac.cn
Y. Zheng
College of Pharmaceutical Sciences
Zhejiang University of Technology
Hangzhou, Zhejiang 310014, China
P. Zhao
College of Materials Science and Engineering
Zhejiang University of Technology
Hangzhou, Zhejiang 310014, China

The ORCID identification number(s) for the author(s) of this article can be found under https://doi.org/10.1002/smll.202307523

DOI: 10.1002/smll.202307523

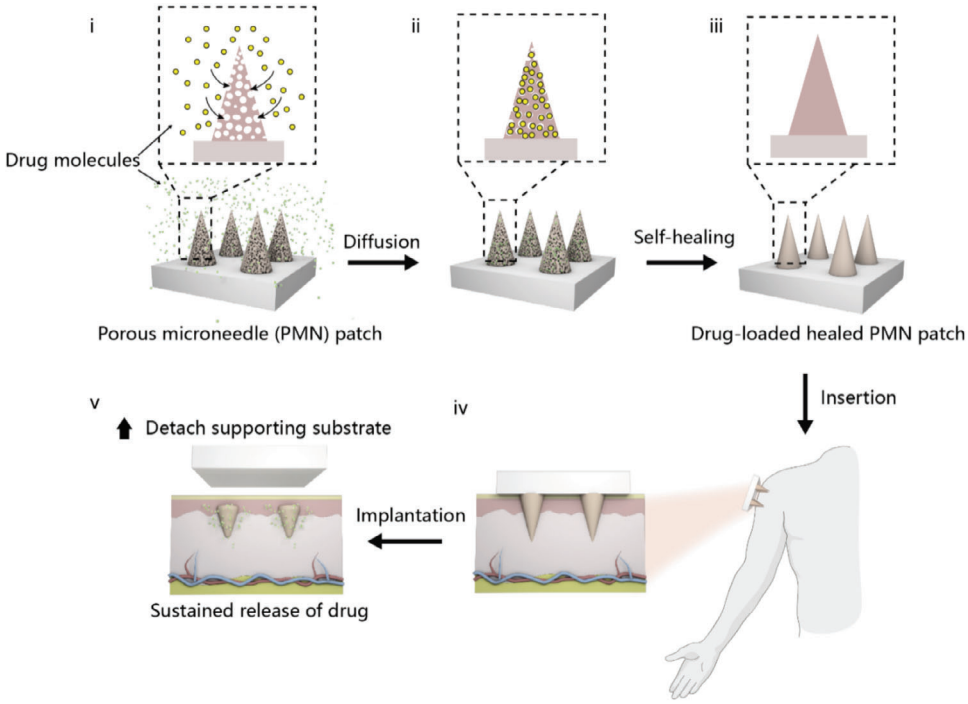

Figure 1. Schematic illustration of drug loading and transdermal administration using self-healing porous microneedle (PMN) patch. i) The proposed PMNs have interpenetrating pores on both the surface and internal areas and are incubated in the aqueous drug solution. ii) Due to the ample space provided by the pores, drug molecules can readily diffuse inside the PMNs, thereby achieving the efficient drug loading. iii) After being exposed to gentle infrared irradiation, the slightly increased temperature (≈43 °C) triggers the glass transition of the polymer material, which leads to the self-healing of the pores. iv) The resulted drug-loaded healed PMN patch can easily penetrate the skin under press. v) By applying a slight shear force with the fingers, the drug-loaded healed PMNs can detach from the supporting substrate and be implanted inside skin tissue, further undergoing gradual biodegradation to achieve sustained drug release.

involves harsh conditions, such as freezing-thaw cycles or UV-irradiation for crosslinking hydrogel and high-temperature or organic solvents for making biodegradable MNs. Such a complicated and harsh process can greatly compromise the bioactivity of loaded drugs, particularly biomacromolecules such as antibodies, peptides, and vaccine antigens.[9] In addition, MNs combined with nano/microparticles are restricted by defects inherent to nano/microparticles, such as low drug loading capacity, potential toxicity, instability, and complexity of manufacturing.[10] These limitations hamper the clinical translation of sustained-release MN delivery systems.

Herein, we introduce a self-healing biodegradable porous microneedle (PMN) patch that not only enables mild and efficient loading of hydrophilic drugs with different molecular weights, but also acts as an implantable drug reservoir for sustained release in a minimally invasive manner (**Figure 1**). The PMN patch consists of an array of porous MNs made from polylactic-co-glycolic acid (PLGA) and a supporting substrate made from a biocompatible resin. The PMN patch is fabricated using a cryogenic micromoulding followed by non-solvent exchange induced phase separation, resulting in interconnected pores on both the surface and internal areas of the MNs (**Figure 2**A). The pores enable PMNs to efficiently load hydrophilic drugs with different molecular weights in a diffusion manner, and they can further be self-healed under mild conditions to form the drug-loaded biodegradable MNs. The healed PMN can efficiently penetrate the skin with a thumb press and detach from the supporting substrate under shear, acting as drug reservoirs implanted into skin tissue. Subsequently, they undergo slow biodegradation in the skin to achieve the sustained release of the payload for over 40 days. The PMN patch was used to load methotrexate (MTX) and ovalbumin (OVA) as a model antigen, followed by transdermal administration. Our results demonstrate that one-time administration of desired therapeutics using healed PMN patch resulted in more robust and durable efficacy in alleviating psoriasis and inducing adaptive immune responses compared to conventional methods with multiple administrations.

2. Results and Discussion

2.1. Design, Fabrication, and Characterization of Self-Healing PMN Patches

PLGA is chosen as the material for the PMNs due to its biodegradability, biocompatibility, and ability to be formulated for sustained drug release over weeks to months.[11] In addition, PLAG endows the PMNs with a self-healing ability, which occurs at temperature near glass transition temperature (T_g) of PLGA, ranging from 30 to 60 °C.[12] During the glass transition of PLGA, its chains undergo rearrangement and self-assembly, which can subsequently result in the healing of pore structures on a macroscopic scale.[13] The supporting substrate was made from a biocompatible resin that is impermeable and hydrophobic. This design effectively prevents the drug from diffusing into the

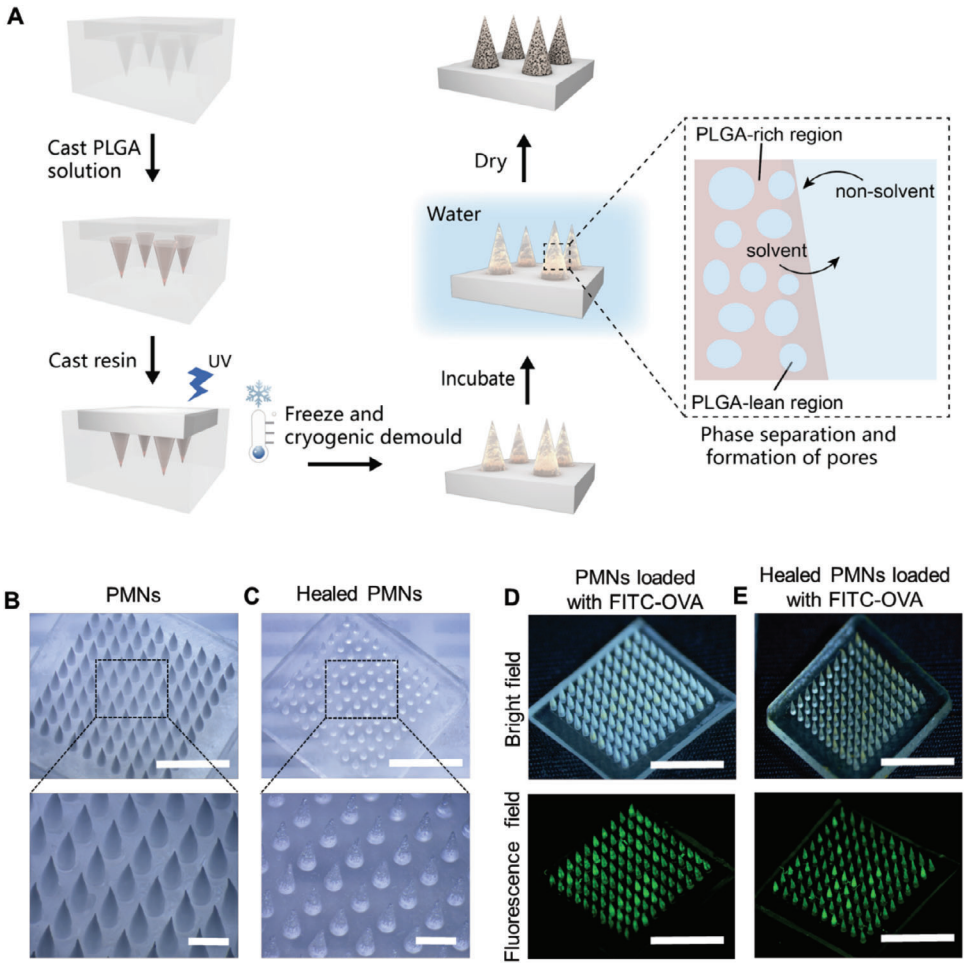

Figure 2. Fabrication and characterization of self-healing PMN patch. A) Schematic illustration of the fabrication process of self-healing PMN patch. The self-healing PMN patch was fabricated using a cryogenic micromoulding followed by phase separation process. Representative bright-field microscopy images of PMN patch B) and healed PMN patch C). Scale bar, 1000 μm (up) and 200 μm (down). Representative bright-field and fluorescence-field microscopy images of FITC-OVA loaded PMN patch D) and healed PMN patch E). Scale bar, 2000 μm.

supporting substrate during the drug loading process. As a result, it improves the efficiency of delivery and reduces the drug waste because only the microneedles can be inserted into the skin. The self-healing PMN patch was fabricated using a cryogenic micromoulding followed by the phase separation process (Figure 2A). Briefly, PLGA solution was poured into the PDMS mould to fill the microneedle cavities. A photo-curable resin was then poured into the remaining sections of the mould, forming the supporting substrate through UV irradiation. The filled PDMS mould was placed at −20 °C for 4 h. After cryogenic demoulding, the resulting MN patch was immersed in deionized water for 4 h to induce pore formation through phase separation. Finally, the PMN patch was obtained after complete drying.

Cryogenic demoulding is a critical step during fabrication. The freezing treatment leads to the formation of ice within MNs, which facilitates the complete removal of the MNs composed of the PLGA solution from the mould while preserving their shape and structural integrity. It is similar to the fabrication of cryomicroneedles.[14] With the increase of phase separation temperature from 4 to 37 °C, accelerating the diffusion rate of solution and the rearrangement of PLGA chains in the MNs. The morphology of MNs is more uniform and complete, and pores are interconnected at 37 °C (Figures S1 and S2, Supporting Information). Moreover, the MNs experienced different degrees of swelling under different temperature conditions, as indicated by an increase in height to approximately 717, 1017, and 1400 μm, respectively, at the temperature of 4, 25, and 37 °C (Figure S4, Supporting Information). In addition, as the concentration of PLGA increased from 200 to 600 mg mL^{-1}, the size of the large pores in the PMNs gradually decreased, while the size of the small pores gradually increased after phase separation at 37 °C. Moreover, at a concentration of 200 mg mL^{-1}, the pores formed on the surface of the PMNs are larger and more densely packed, which hinders closure. Additionally, at a concentration of 600 mg mL^{-1}, the pores formed are too small, which will adversely affect the drug load (Figure S3, Supporting Information). However, at a concentration of 400 mg mL^{-1}, the color of the MNs changed to a pale white, and they exhibited a "sponge-like" morphology (refer to Figure S5B,E, Supporting Information). After cryogenic demoulding, the obtained MNs were translucent,

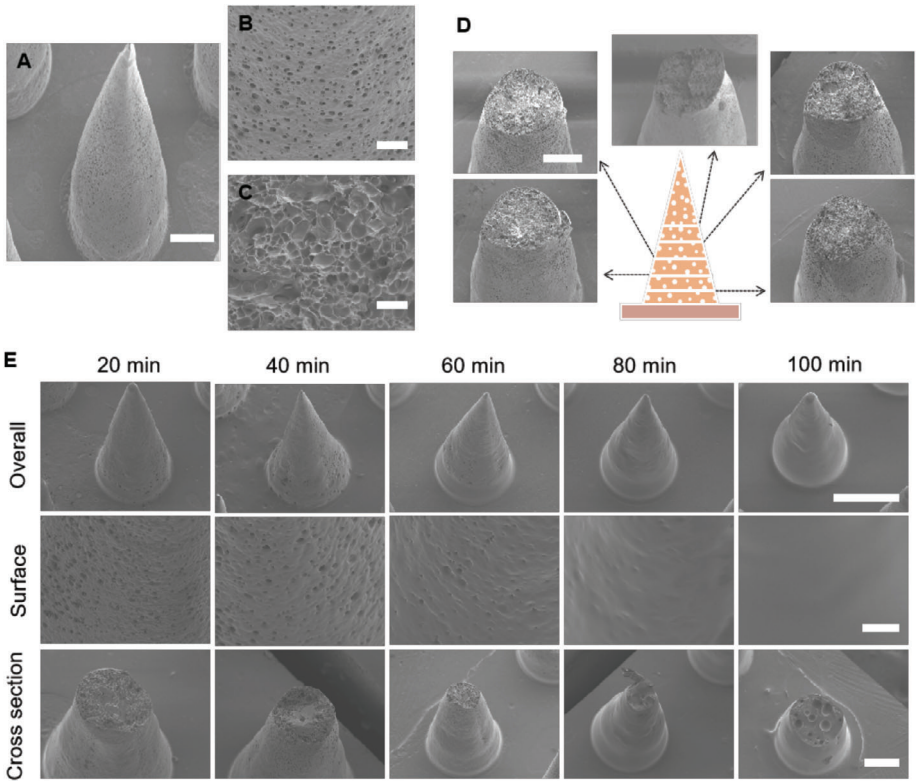

Figure 3. Morphology of PMN patch and healed PMN patch. Representative SEM images of overall PMNs A), scale bar, 200 μm, surface of PMNs B), scale bar, 20 μm, and the cross section of PMNs C), scale bar, 20 μm. D) Representative SEM images of cross sections of PMNs at different heights, Scale bar, 200 μm. E) Representative SEM images of overall healed PMNs at different IR irradiation times, scale bar, 500 μm, as well as their surface, scale bar, 20 μm, and the cross sections, scale bar, 100 μm.

with a height of approximately 1200 μm (Figure S5A,E, Supporting Information). The dimensions of the MNs after cryogenic demoulding are similar to those of the MN master template, indicating successful replication of the template. Additionally, cryogenic demoulding allowed the MNs to retain the solvent phase, which resulted in immediate phase separation within the MNs upon immersion in the non-solvent (i.e., water). Due to the miscibility of the solvent (1,4-dioxane) and the non-solvent (water), an exchange occurred between the solvent and non-solvent, leading to the formation of polymer-rich and polymer-lean phases. After thorough drying, the polymer-rich phase establishes the skeletal structure of the PMNs, while the polymer-lean phase creates the pores.[15]

The fabricated PMN patch comprised a 10 × 10 array of vertically arranged porous microneedles on a transparent resin supporting substrate (Figure 2B). Scanning electron microscopy (SEM) images revealed that the PMNs have a relatively uniform size and that their surfaces are uniformly distributed with pores ranging in diameter from 5 to 10 μm (**Figure 3**A,B). The cross-section of MNs at various heights was further demonstrated to possess numerous external pores and internally interconnected cavities, which were formed through swelling and phase separation (Figure 3C,D; Figure S6, Supporting Information). The sizes of the pores from 5 to 10 μm are sufficient for loading both low and high molecular weight drugs.[16]

The PMNs were exposed to the gentle infrared (IR) irradiation to increase the temperature to ≈43 °C (Figure S7A,B, Supporting Information), resulting in the self-healing of pores on both the surface and within the internals of the MNs (Figure 3E). This temperature was also applied for sealing PLGA in previous study.[17] In addition, the degree of pore healing increases with the duration of IR irradiation. When the irradiation time reached 80 min, the pores inside and on the surface of the MNs were completely healed, despite the fact that the internal air could not be fully expelled during the glass transition of PLGA (Figure 3E). After complete healing of pores, the color of MNs transformed from white to semi-translucent (Figure 2C), and the MNs reduced in size to ≈1000 μm in height (Figure S5C,E, Supporting Information). After separating the MNs from the supporting substrate, it is observed that the MNs are connected to a supportive cap structure with a height of ≈300 μm (Figure S5D,E, Supporting Information). Therefore, the actual height of the healed PMN is ≈700 μm. This phenomenon may arise from the rearrangement of molecular chains caused by the movement of polymer chains during the process of glass transition, leading to a reduction in the volume of MNs.[18]

2.2. Mechanical Performance and Skin Insertion Ability of PMN Patch

Sufficient mechanical strength is crucial for successful skin penetration by MNs. The mechanical strength of the PMN patch was

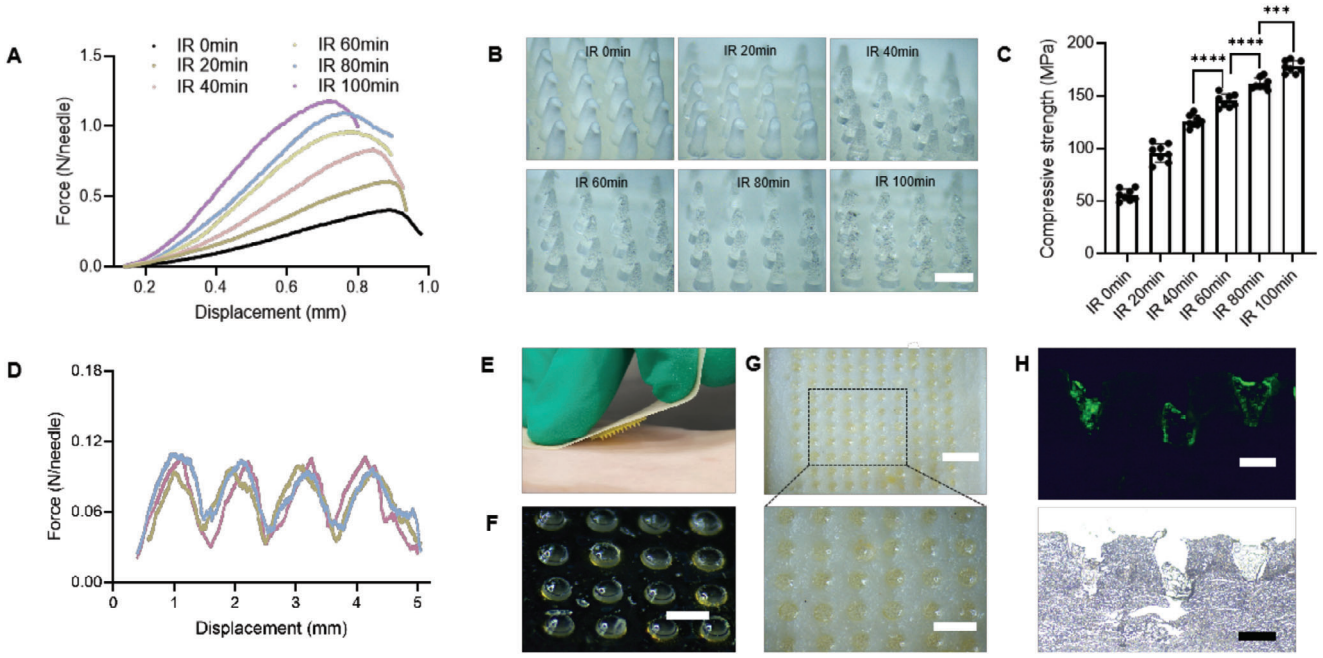

Figure 4. Mechanical property of healed PMN patch. A) Schematics of the experimental were obtained for the healed PMN patch exposed to different IR irradiation times under vertical compression force. Data are presented as means ± s.d. ($n = 8$ independent samples). B) Representative images of healed PMN patches irradiated at different IR times after vertical pressure. Scale bar, 1000 μm. C) Compressive strength of healed PMN patch prepared by IR irradiation at different times. Data are presented as means ± s.d. ($n = 8$ independent samples). D) Schematic of the mechanical experimental for the healed PMN patch under compression applied by a horizontal force after an 80 min period of IR irradiation. Data are presented as means ± s.d. ($n = 3$ independent samples). E) Representative photographs of healed PMNs loaded with FITC-OVA before inserted into the fresh porcine skin. F) The separated substrate of FITC-OVA loaded healed PMNs after being inserted into the porcine skin. Scale bar, 500 μm. G) Representative images of needle retention in porcine skin after insertion of FITC-OVA loaded healed PMNs. Scale bar, 200 μm. H) Representative images of cryosections after application of FITC-OVA loaded healed PMNs inserted into the porcine skin. Scale bar, 500 μm. In C, ***$p < 0.001$ versus IR 80 min, ****$p < 0.0001$ versus IR 60 min, ****$p < 0.0001$ versus IR 40 min.

assessed using a tensile testing machine after different durations of IR irradiation. The load versus displacement profiles showed that the force of PMNs could tolerate increased, while the fracture or bend displacement decreased with longer IR irradiation time (**Figure 4**A). This result indicates that the rigidity of PMNs increased while their toughness decreased with the increasing intensity of the glass transition of the PMNs. Regardless of whether the PMNs healed, they were able to withstand compressive forces greater than 0.3 N per needle without fracturing or bending. This force is higher than the minimum average force required for normal skin penetration, which is 0.058 N per needle.[19] As the irradiation time increases, the morphology of PMNs undergoes a significant phase transition from a white appearance to a translucent one during compression (Figure 4B). Additionally, the degree of bending or breaking displacement gradually decreases. The compression strength was calculated from the slope of stress-strain curve. After subjecting the PMNs to IR irradiation for various durations (0, 20, 40, 60, 80, and 100 min), the compression strengths were measured as follows: 55.9 ± 7.6, 95.7 ± 11.2, 126.1 ± 9.5, 145.3 ± 10.1, 161.6 ± 9.1, and 177.6 ± 7.9 MPa, respectively (Figure 4C). After subjecting the PMNs to 80 min of IR irradiation, we observed complete healing of both the external and internal pores (Figure 3E). Additionally, the compressive strength reached a satisfactory level (Figure 4A). Based on these results, we selected this duration as the optimized healing time for subsequent experiments. Importantly, we also found no significant difference in the OVA content loaded in the PMN patch before and after IR-irradiation for 80 min (Figure S7C, Supporting Information), which suggests that this healing process did not affect the activity of OVA.

Moreover, shear fracture strength of PMNs after 80 min of healing was determined under shear administrated by a horizontal force. The healed PMNs easily separated from the backing under a shear force of ≈0.11 N per needle (Figure 4D), which can be easily applied by hand.[20] To evaluate the skin insertion capability of the healed PMNs, we used a healed PMN patch containing FITC-OVA for visualization and applied it to porcine skin, which is anatomically similar to human skin (Figure 4E).[21] The healed PMNs were inserted into the skin by applying thumb pressure and left in place for ≈30 s. Subsequently, a gentle shear force was applied with the finger for 5 s to detach the MNs from the supporting substrate. The MNs achieved a 100% insertion ratio, as confirmed by an array of spots (10 × 10) and dye color of FITC-OVA on the skin surface (Figure 4G). Minimal FITC-OVA residue (light yellow) was observed on the resin supporting substrate (Figure 4F). Histological sections revealed that the healed PMNs were completely embedded in the skin tissue after separation from the substrate (Figure 4H). The complete implantation of microneedles within the skin can be attributed to the supportive cap structure on the backing (Figure S5D, Supporting Information), which enhances the penetration depth of the MNs. This excellent penetration ability and the implantable features of

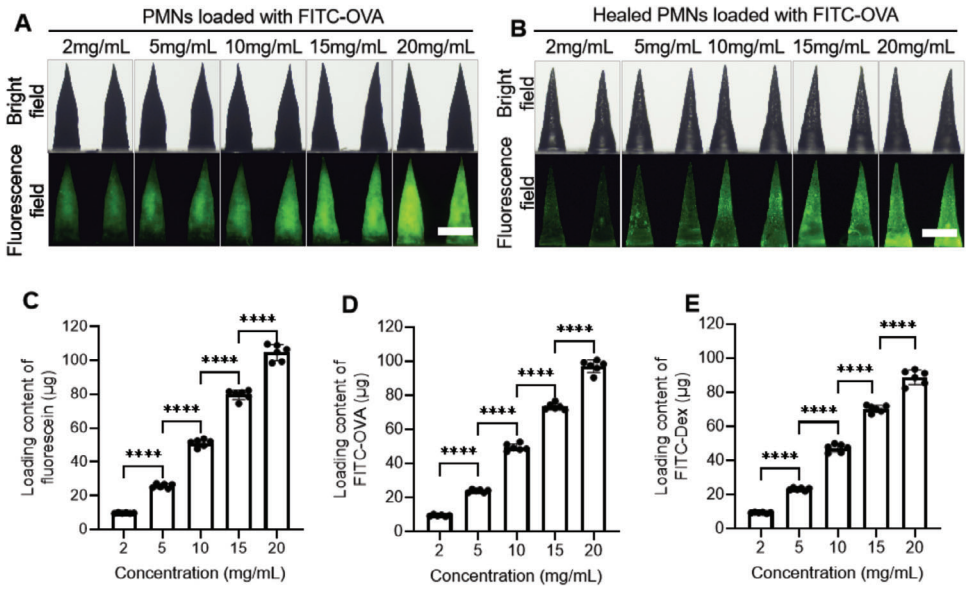

Figure 5. Drug loading capacity of self-healing PMN patch. Representative bright-field and fluorescence-field microscopy images of PMNs A) and healed PMNs B) loaded with FITC-OVA at the concentration of 2, 5, 10, 15, and 20 mg mL^{-1}. Scale bar, 500 μm. Loading capacity of PMNs with C) fluorescein (376 Da), D) FITC-OVA (45 kDa), and E) FITC-Dex (150 kDa) at various concentrations. Data are presented as means ± s.d. (n = 6 independent samples). In C, D, and E, ****p < 0.0001 versus 15 mg mL^{-1}, ****p < 0.0001 versus 10 mg mL^{-1}, ****p < 0.0001 versus 5 mg mL^{-1}, ****p < 0.0001 versus 2 mg mL^{-1}.

healed PMN patch would potentially improve drug delivery efficiency by reducing drug leakage from the skin.

2.3. Drug Loading Capacity of the PMN Patch

Due to the existence of numerous external open pores and internally interconnected cavities, the drug molecules can be loaded into the PMNs through the diffusion effect during the incubation process (Figure 1). To evaluate the drug loading capacity of PMN patch, we utilized three model drugs with varying molecular weights: fluorescein (376 Da), fluorescein isothiocyanate-labelled ovalbumin (FITC-OVA, 45 kDa), and fluorescein isothiocyanate-labelled dextran (FITC-Dex, 150 kDa). Each drug was loaded into the PMN patch individually, employing different concentrations of incubation solution (2, 5, 10, 15, and 20 mg mL^{-1}). All types of drugs were successfully loaded into the PMN patch through diffusion, as evidenced by the distribution of the fluoresce signal along with the MN matrix (**Figure 5**A,B; Figure S8, Supporting Information). The fluorescence intensity of FITC-OVA and FITC-Dex in PMNs increased as the concentrations of incubation solution increased (Figure 5A,B; Figure S8C,D, Supporting Information). However, we observed that as the concentration of the incubation solution increased, the fluorescence intensity of fluorescein in PMNs gradually decreased to the point where it was no longer clearly visible (Figure S8A,B, Supporting Information). This decrease can be attributed to the high concentration of fluorescein, which causes molecular collisions, reduces the fluorescence efficiency of the molecules, and ultimately leads to the phenomenon of fluorescence self-extinction.[22] Using FITC-OVA as an example, the morphology of both the PMN patch and the healed PMN patch after drug loading shows that FITC-OVA was predominantly concentrated within the needle parts and minimal fluorescence was observed in the resin supporting substrate (Figure 2D,E), which would potentially avoid drug waste and improve delivery efficiency.

Furthermore, the loading content of fluorescein, FITC-OVA, and FITC-Dex using PMN patch were quantified, respectively. The loading content is positively correlated with the concentration of the incubation drug solution, regardless of the drugs' molecular weight (Figure 5C–E). When the concentration of the incubation solution was 2, 5, and 10 mg mL^{-1}, the loading content of the three drugs in PMNs was the same, ≈10, 22, and 44 μg, respectively. At concentrations of 15 and 20 mg mL^{-1} in the incubation solution, the drug loading content of PMNs slightly decreased as the molecular weight of the drugs increased. For instance, when the concentration of the incubation solution was 20 mg mL^{-1}, the loading content of PMNs for fluorescence, FITC-OVA, and FITC-Dex was 104.5 ± 5.1, 97.1 ± 3.7, and 88.9 ± 4.7 μg, respectively. Anyway, these results suggest that the PMN patch was able to load hydrophilic drugs, ranging from small molecules to large molecules, through diffusion. The post-loading approach, which utilizes the self-healing properties of materials, has also been employed in the development of sustained release microcapsules, also demonstrating great advantages compared to the pre-loading approach.[13,23] Additionally, the loading content could be precisely controlled by adjusting the drug concentration in the incubation solution.

2.4. Drug Release and Degradation of Healed PMN Patch

FITC-OVA was loaded into the PMNs for the studies of release kinetics and degradation behavior. The MNs were incubated in

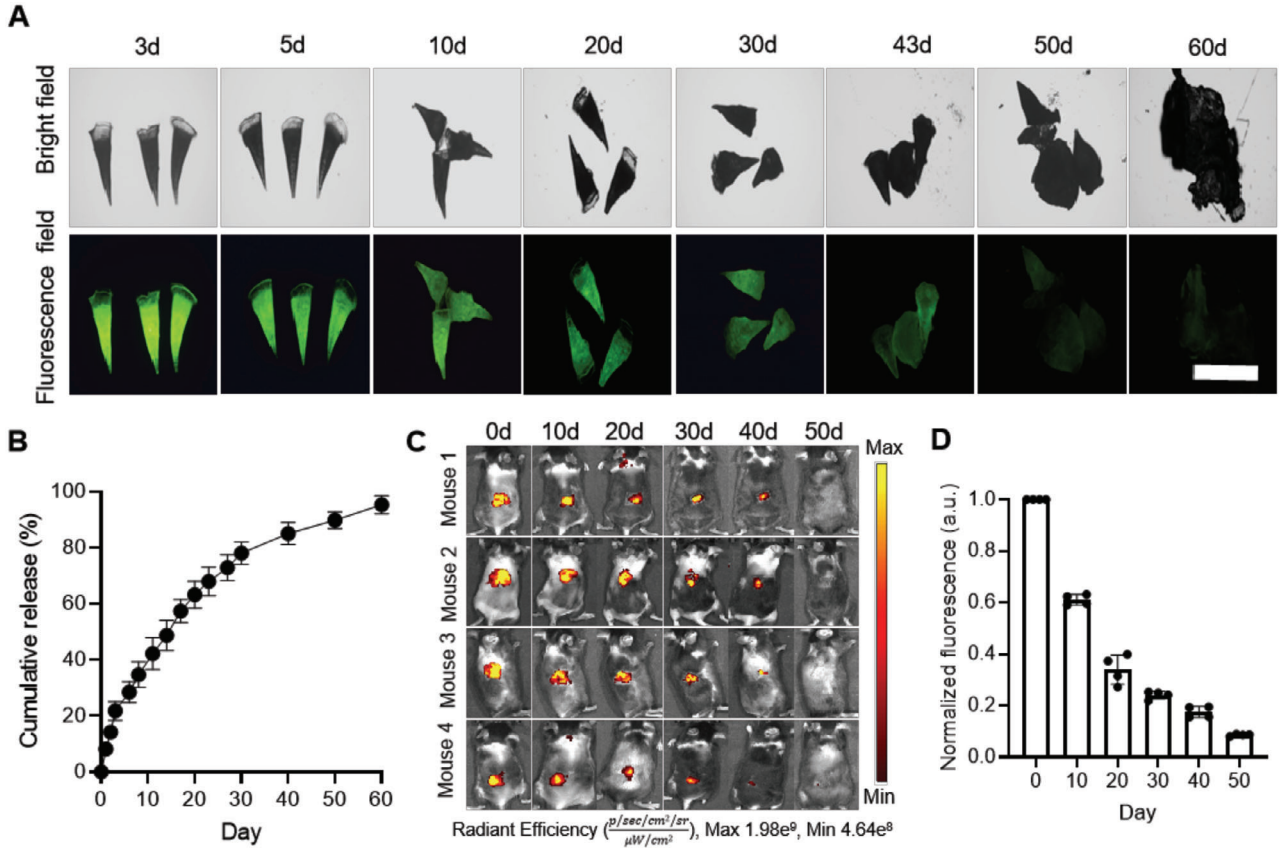

Figure 6. In vitro and in vivo degradation and drug release of healed PMN patch. A) Representative bright-field and fluorescence-field microscopy images of the degradation behaviour of FITC-OVA loaded healed PMNs on day 3, 5, 10, 20, 30, 43, 50, and 60 in vitro. Scale bar, 1000 µm. ($n = 6$ independent samples). B) The cumulative release of OVA-loaded healed PMNs was measured with a BCA kit during two months of incubation in vitro. Data are presented as means ± s.d. $n = 6$ independent samples. C) Optical images taken from IVIS analysis demonstrated the release of FITC-OVA-loaded healed PMNs embedded inside the skin of the mice over a long period of time. ($n = 4$ independent animals). D) Quantification analysis of fluorescence intensity was performed on IVIS images to measure the persistence of FITC-OVA loaded healed PMNs embedded inside the skin of mice over an extended period. Data are normalized to the fluorescence intensity at day 0. Data are presented as means ± s.d. ($n = 4$ independent animals).

phosphate-buffered saline (PBS, pH 7.4) at 37 °C to mimic the physiological environment. We first examined the morphological changes of healed PMNs during the degradation and the long period of FITC-OVA release. As shown in **Figure 6**A, the MNs immersed in PBS for a duration of 5 days exhibited a sharp-pointed conic shape and displayed a strong fluorescence intensity. However, the tips of MNs were passivated, and the MNs gradually expanded while the fluorescence intensity slowly decreased after being immersed in PBS from 10 to 30 days. The MNs displayed a poor appearance and low fluorescence intensity after being immersed for 43 days. It took 60 days for the MNs to degrade almost completely and the fluorescence signal was almost invisible. The observed phenomenon of degradation may be attributed to the pore formation and erosion caused by PLGA during hydrolysis, leading to an increased volume and slow release of FITC-OVA.[24] Furthermore, the cumulative release of OVA from healed PMNs was quantified. There was almost no burst release of OVA on day 1 (Figure S9, Supporting Information), and most of the drug (≈96.2 ± 3.5%) was gradually released from the MNs over 60 days (Figure 6B).

To evaluate the in vivo drug release, we monitored the fluorescence signal of FITC-OVA after its delivery into the mice's back skin using healed PMN patch. Once the MNs implanted into skin, a strong fluorescence signal was observed on the site of administration (Figure 6C,D). Once the healed PMNs punctured into the skin, the fluorescence signal and intensity can be captured at day 0. With the microneedles embedded in the skin for an extended period, the fluorescence signal and intensity gradually diminished. The fluorescence signal gradually weakened from the center to the outer edges of application sites due to the diffusion of FITC-OVA released from the healed PMNs. After 50 days, there was nearly no fluorescence signal detected. The degradation and OVA release of healed PMNs show slight differences between in vivo and in vitro settings, which might be attributed to the more complex physiological environment of the skin compared to PBS. For example, the presence of enzymes in the skin resulted in an enzyme-catalyzed degradation mechanism of PLGA, which differs from pure hydrolytic degradation.[25] Anyway, these results collectively indicate that the healed PMN patch has the capability to achieve a delivery timeframe of at least one and a half months. Long-acting drug delivery formulations that facilitate sustained drug release are highly preferable in many clinical therapies by prolonging therapeutic effects, minimizing systemic toxicity, and enhancing patient adherence.[26] The

healed PMNs can be easily detached from the supporting substrate once inserted into the skin (Figure 4G). This implantable feature not only minimizes discomfort caused by long-term patch wearing on the skin surface but also has the potential to protect patients' medication privacy.[9a]

2.5. Sustained Delivery of Therapeutics by Healed PMN Patch in Treatment of Psoriasis

Psoriasis is a chronic, immune-mediated inflammatory skin disease characterized by erythema, desquamation, and thickening. It has a significant impact on the physical and mental health of patients.[27] Methotrexate (MTX) has long been considered the first-line pharmacotherapy for psoriasis, but it is associated with systemic side effects such as nausea, vomiting, neutropenia, and hepatotoxicity.[28] To evaluate the therapeutic effects of MTX-loaded healed PMN patch, a mouse model of psoriasis induced by imiquimod (IMQ) on the mice dorsal skin was established. The oral and topical administration of MTX were used for comparison. The release profile of MTX is similar to that of OVA from healed PMNs (Figure S10, Supporting Information). About 60% of MTX was gradually released from the MNs over the course of 20 days. The schedules of different administration methods are illustrated in **Figure** 7A. The skin lesions of mouse with IMQ-induced psoriasis generally exhibited typical manifestations of erythema, induration, and thickening.[29] On day 7, psoriasis-like lesions were observed in the model group and blank MN treated group, displaying severe hyperkeratosis (Figure 7B). One-time administration of MTX with healed PMNs greatly improves the severity of psoriasis in IMQ-induced skin lesions, compared to oral and topical administration, even with increased administration frequency. The severity of the disease was assessed daily using an objective scoring system called the Psoriasis Area and Severity Index (PASI), which is based on the evaluation of erythema, scaling, and induration. The psoriasis lesion area and PASI scores observed over the 7-day period were consistent with the pathological symptoms depicted in the images and statistical data on skin thickness. This indicates that the overall efficacy of administering MTX-loaded healed PMN patches is superior to that of other treatment groups (Figure 7C; Figure S11A, Supporting Information). Topical application of IMQ can induce splenomegaly in mice due to the increase infiltration of immune cells such as dendritic cells, macrophages, and T cells.[30] The spleens of the model mice that did not receive MTX treatment displayed the largest size and the highest weight. The administration of MTX with healed PMN patches can reverse splenomegaly, resulting in a smaller and lighter spleen compared to oral and topical administration (Figure 7E,F).

The severity of psoriasis was further determined by weighing the skin biopsy specimens. The weight of the skin biopsy from the mice treated with MTX-loaded healed PMN patch was significantly lower than that of the mice treated with oral and topical administration (Figure 7D). The full-thickness skin of mice was subjected to H&E (hematoxylin and eosin) staining. H&E staining revealed severe hyperkeratosis in both the model group and the blank healed PMN group, which was characterized by epidermal hyperplasia and edema. The epidermal thickness of mice treated with MTX-loaded healed PMNs is 39.82 ± 3.74 μm (Figure 7G,H). In comparison, mice that received oral or topical administration, regardless of the number of administrations, showed a thicker epidermis. The thickness measured was 124.43 ± 3.94 μm for oral administration once, 100.64 ± 2.71 μm for oral administration three times, 129.39 ± 2.63 μm for topical administration once, and 106.12 ± 3.65 μm for topical administration three times, respectively (Figure 7G,H). The level of glutamic oxaloacetic transaminase (GOT) in the liver was evaluated to assess the systemic side effects of different treatments because the liver is responsible for metabolizing drugs. Oral administration of MTX induced the higher level of GOT than topical and MN administration. Increasing the topical administration times resulted in upregulation of GOT level. One-time administration MTX with healed PMN patches did not cause substantial harm (Figure 7I). Meanwhile, no obvious change in body weight was monitored during treatment (Figure S11B, Supporting Information). Collectively, the data demonstrate that a single dose of MTX-loaded healed PMN patch has been shown to achieve prolonged therapeutic effects in the mitigation of psoriasis while minimizing side effects, even compared to multi-dose via oral and topical administration.

2.6. Sustained Delivery of Antigens with Healed PMN Patch Elicit Potent and Durable Adaptive Immune Responses

To describe the application in vaccination, we applied the PMN patch to loaded the OVA, a widely used model vaccine antigen,[31] and compared the humoral and cellular immune responses with conventional vaccination approaches including subcutaneous (SC) and intramuscular (IM) injections. Mice received single vaccination on day 0 and the sera samples were collected on day 0, 10, 20, and 30 (**Figure** 8A). The levels of OVA-specific IgG and IgG1 induced by the OVA-loaded healed PMN patch were significantly higher compared to those in the SC and IM injection groups (Figure 8B,C). These levels showed a continuous increase over a period of 30 days. This data implies the sustained delivery of antigen with healed PMNs induced stronger humoral immune responses than SC and IM injection. Furthermore, the antigen-specific cellular immune responses induced by different vaccination methods were evaluated. Compared to SC and IM injections, vaccination with OVA-loaded healed PMNs resulted in higher levels of OVA-specific IgG2a antibody (Figure 8D), suggesting enhanced cell-mediated immune response.[32] Splenocytes of mice vaccinated with OVA-loaded healed PMNs showed the fastest proliferation (Figure 8E) and secreted higher levels of IFN-γ (Figure 8F) compared with those from mice vaccinated with OVA-SC and OVA-IM injection groups. The OVA-specific cytotoxic T lymphocyte (CTL) immunity relied on the ratio of effector cells to target cells. Specifically, it determined the specific killing effect between splenic T lymphocytes from vaccinated mice and the B16 melanoma cell line transfected with ovalbumin (OVA-B16). The data indicates a significant increase in the efficiency of inducing OVA-B16 cell lysis as the proportion of splenocytes increased from 10:1 to 100:1. Additionally, OVA-loaded healed PMNs demonstrated higher lysis efficiency compared to OVA injections via IM and SC methods (Figure 8G). Finally, after being vaccinated with OVA-loaded healed PMNs,

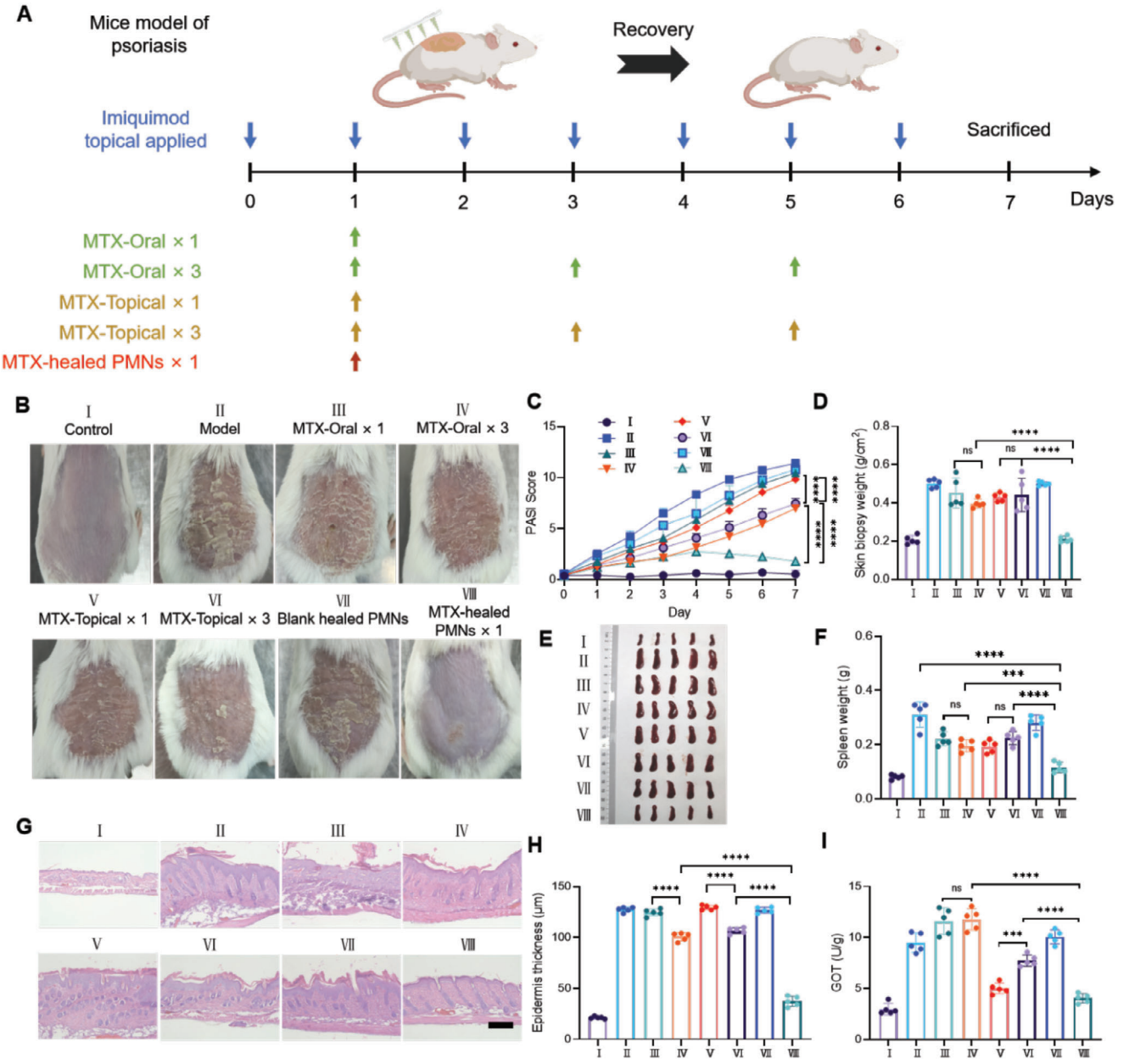

Figure 7. Psoriasis alleviation by methotrexate (MTX)-loaded healed PMN patch. A) Schematic illustration of different treatments for imiquimod (IMQ)-induced psoriasis. B) Representative photographs of imiquimod-induced psoriasis mice treated with various treatments on day 7. C) PASI score of psoriasis skin. D) The punch biopsy weight in the back skin of psoriasis mice after the indicated treatments on day 7. E) The images of spleen harvested on day 7. F) Spleen weights of experiment mice on day 7. G) H&E staining of skin tissue sections after treated with various formulations. Scale bar, 200 μm. H) Quantification of epidermal thickness in H&E-stained microphotographs. I) Glutamic Oxalacetic Transaminase (GOT) activity in mice liver was determined by GOT/AST kit after various treatments. The code demotes the following: I, Control (health mice without psoriasis); II: Model (psoriasis mice without treatment); III: MTX-Oral×1 (psoriasis mice with oral administration of MTX one time); IV: MTX-Oral×3 (psoriasis mice with oral administration of MTX three times); V: MTX-Topical×1 (psoriasis mice with topical administration of MTX one time); VI: MTX-Topical×3 (psoriasis mice with topical administration of MTX three times); VII: Blank healed PMNs (psoriasis mice treated with blank healed PMNs); VIII: MTX-healed PMNs×1 (psoriasis mice treated with MTX-loaded healed PMNs one time). Data are presented as means ± s.d. ($n = 5$, independent animals). Two-tailed Student's *t*-test was used to compare MTX-Oral×1, MTX-Oral×3, MTX-Topical×1, and MTX-Topical×3 groups. In C, ****$p < 0.0001$ versus MTX-Oral×3 group, ****$p < 0.0001$ versus MTX-Topical×3 group. In D, ****$p < 0.0001$ versus MTX-Oral×3 group, ****$p < 0.0001$ versus MTX-Topical×3 group, $p > 0.05$ versus MTX-Topical×1 group, $p > 0.05$ versus MTX-Oral×1 group. In F, ****$p < 0.0001$ versus MTX-Oral×3 group, ****$p < 0.0001$ versus MTX-Topical×3 group, ****$p < 0.0001$ versus Model group, $p > 0.05$ versus MTX-Topical×1 group, $p > 0.05$ versus MTX-Oral×1 group. In H, ****$p < 0.0001$ versus MTX-Oral×3 group, ****$p < 0.0001$ versus MTX-Topical×3 group, ***$p < 0.001$ versus MTX-Topical×1, ****$p < 0.0001$ versus MTX-Oral×1 group. In I, ****$p < 0.0001$ versus MTX-Oral×3 group, ****$p < 0.0001$ versus MTX-Topical×3 group, ***$p < 0.001$ versus MTX-Topical×1, $p > 0.05$ versus MTX-Oral×1 group. In G, three images were taken for each group and all experiments were repeated independently twice, with similar results.

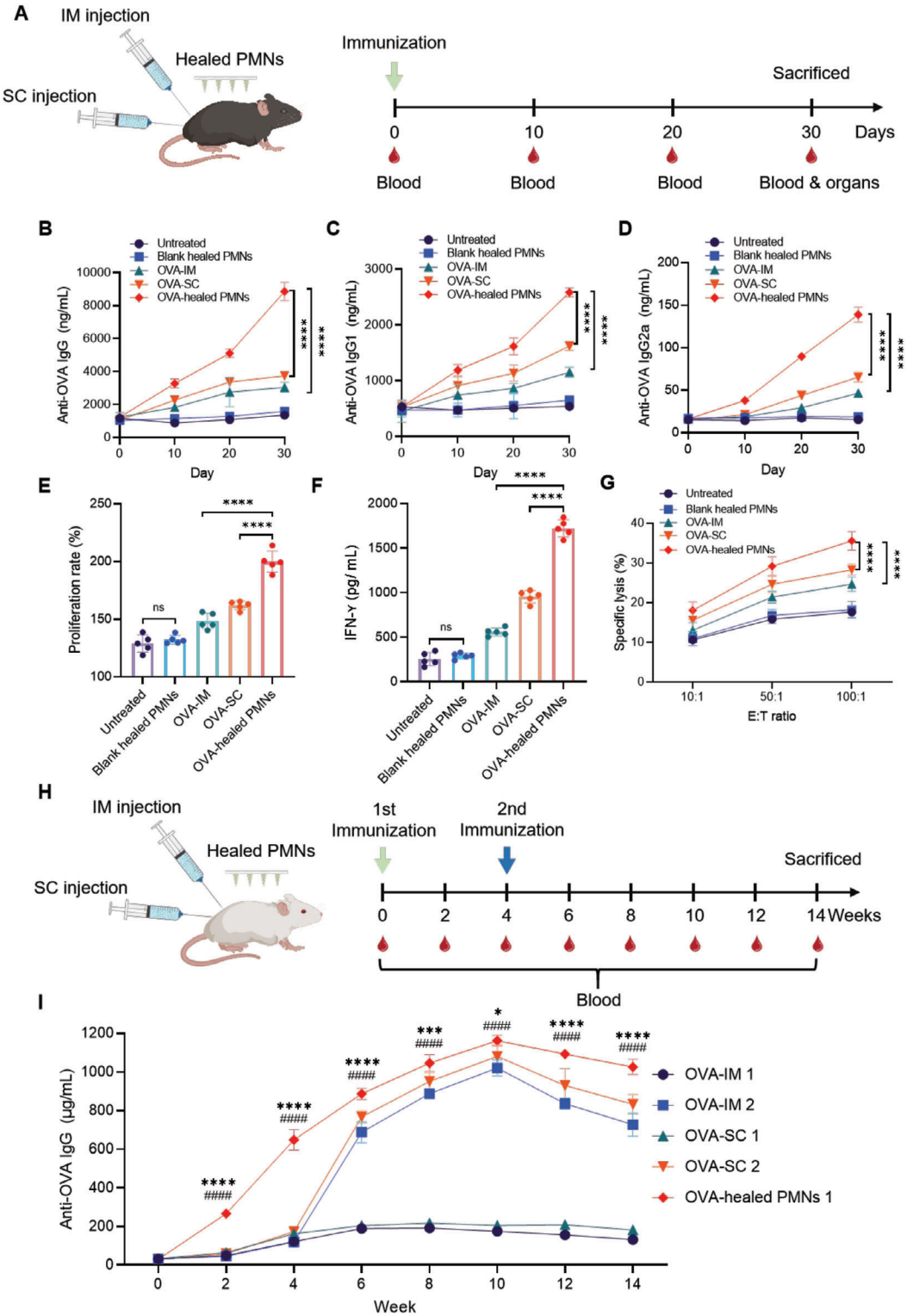

Figure 8. Vaccination of antigen (OVA)-loaded healed PMN patch. A) Schematic illustration of different vaccination methods on day 0. Vaccination with OVA-healed PMNs (OVA-loaded healed PMNs), subcutaneous (OVA-SC), and intramuscular (OVA-IM) injections of OVA, and blood was collected on days 0, 10, 20, and 30. The level of anti-OVA IgG B), IgG1 C), and IgG2a D) antibodies by ELISA over time. E) In vitro proliferation of extracted splenocytes restimulated with 50 μg mL^{-1} antigen (OVA). The proliferation rate of splenocytes at 72 h was relative to 0 h and was obtained using CCK-8 assay. F) Secretion level of IFN-γ in the culture supernatants after 72 h of culture. G) Determination of cytotoxic T lymphocyte (CTL) activity in vitro. Effector cells (splenocytes) and target cells (B16-OVA cells) were co-cultured at different ratios. "E:T" refers to the ratio of effector cells (E) and target cells (T).

the weight of mice was not affected (Figure S12, Supporting Information), and there were no abnormalities observed in the main organs (heart, spleen, liver, kidney, and lung) (Figure S13, Supporting Information).

Finally, we assessed the duration of immune responses following a single administration of OVA using a healed PMN patch and conducted a longitudinal analysis of antigen-specific IgG production following various vaccination protocols (Figure 8H). For a single bolus injection via SC or IM route, a delayed OVA-specific humoral immune response was observed after 4 weeks following immunization and it gradually decayed after the 6th week (Figure 8I). The second immunization of OVA via SC or IM injection induced a significant increase in level of OVA-specific IgG antibody at week 6 (4 weeks after the second immunization). The level of IgG antibody, using the double immunization regimens, began to wane at the 10th week. A single immunization of OVA using the healed PMN patch results in a significant increase in the level of OVA-specific IgG antibodies in the 2nd week and maintains this trend until the 10th week. Although the level of IgG antibodies using the healed PMN patch started to wane from the 10th week, the values still remained higher over time compared to those after double immunization regimens via SC and IM injections. In the 14th week after the first immunization, the levels of OVA-specific IgG, IgG1, and IgG2a antibodies were significantly higher when using the OVA-loaded healed PMN patch compared to double SC or IM injections (Figure S14, Supporting Information). These results collectively indicate the capability of a healed PMN patch to not only induce more robust but also longer-lasting antigen-specific adaptive immune responses, compared to conventional bolus injections via SC and IM routes. The enhanced and prolonged immunity can be attributed to two factors: the spatial factor and the temporal factor. From a spatial perspective, the antigen is delivered into the skin, which is rich in antigen-presenting cells (APCs) critical for initiating an adaptive immune response.[2a] From a temporal perspective, the sustained release of antigen can prolong the exposure and presentation of the antigen, similar to natural infections.[2b] This painless, easy-to-use, efficient, and single-administration vaccination strategy could be an attractive alternative for mass vaccination programs, especially during a pandemic. The applications of the PMN patch are not limited to treating psoriasis and vaccination. By loading desired therapeutics, this PMN patch could be used for various clinical purposes where there is a need for long-acting medication, such as contraception, suppression of androgens, and the treatment of opioid and alcohol addiction.[1a]

3. Discussion

Porous MNs have been explored for drug and cell delivery.[33] However, none of the existing systems has been demonstrated to achieve sustained delivery of loaded therapeutics, and they always experience rapid release due to the leakage of the loaded therapeutics from the pores.[33a,b] To the best of our knowledge, our PMN patch with self-healing features, specially designed for the sustained delivery of therapeutics, has never been reported before. Currently, several strategies are commonly employed for fabricating porous MNs, including lyophilization, sacrificial porogens, and template phase separation.[33a,b,34] However, the MNs produced through these methods often suffer from structural collapse and low porosity issues.[34a,35] Moreover, both the MNs and their supporting substrate contain pores, which poses a potential risk of drug wastage, as only the drugs loaded in the MN part can be effectively delivered into the skin. In this study, we present a novel fabrication strategy for the PMN patch. The strategy involves a cryogenic demoulding-based micromoulding technique, followed by non-solvent exchange-induced phase separation. The resulting PMNs exhibited well-replicated morphology, and both the surface and interior of the PMNs displayed uniformly distributed interconnected pores (Figures 2 and 3). Besides, the supporting substrate is made of biocompatible and impermeable resin, which ensure the drugs are loaded only in the MN parts (Figures 2 and 5). Long-acting drug delivery formulations that facilitate sustained drug release are highly preferable in many clinical therapies by prolonging therapeutic effects, minimizing systemic toxicity, and enhancing patient adherence.[26] The pores with a self-healing feature enable PMNs to encapsulate hydrophilic drugs with varying molecular weights under gentle conditions. The healed PMN patch facilitates the sustained release of therapeutics, potentially achieving the targeted delivery timeframe of at least one month (Figure 6).

Although promising, several works remain before translating our PMN patch from bench to clinic. First, the specific target release times need to be optimized for different clinical purposes. Since PLGA with varying molecular weights or different proportions of lactic acid and glycolic acid exhibit different degradation rates,[12,36] we can use appropriate PLGA to make PMN patch with the desired release duration. Second, the drug loading capacity of PMNs is still limited due to their micro-scale dimensions, which poses a critical issue when a high dose of drugs is required to achieve an effective therapeutic window. One solution to increase the dosage is by increasing the number of microneedle arrays with a larger patch.[37] Third, developing an applicator is necessary for the reliable administration of the PMN

H) Schematic illustration of different vaccination methods to determine long-term immunity. The first immunization vaccination was performed with subcutaneous injection of OVA (OVA-SC 1), intramuscular injection of OVA (OVA-IM 1), and OVA-loaded healed PMNs (OVA-healed PMNs 1) on week 0. The second vaccinations were performed with subcutaneous injections of OVA (OVA-SC 2) and intramuscular injections of OVA (OVA-IM 2) on week 4. Blood of experiment mice was collected on week 0, 2, 4, 6, 8, 10, 12, and 14. I) Long-term immunity responses, shown are ELISA analyses of anti-OVA IgG over times. In B-I, data are presented as means ± s.d. ($n = 5$, independent animals). Two-tailed Student's t-test was used to for comparing OVA-SC, OVA-IM, OVA-SC 2, and OVA-IM 2 groups. In (B–G), $^{****}p < 0.0001$versus OVA-SC group, $^{****}p < 0.0001$ versus OVA-IM group. In I, $^{****}p < 0.0001$ versus OVA-SC 2 group and $^{\#\#\#\#}p < 0.0001$ versus OVA-IM 2 group on week 2, $^{****}p < 0.0001$ versus OVA-SC 2 group and $^{\#\#\#\#}p < 0.0001$ versus OVA-IM 2 group on week 4, $^{****}p < 0.0001$ versus OVA-SC 2 group and $^{\#\#\#\#}p < 0.0001$ versus OVA-IM 2 group on week 6, $^{***}p < 0.001$ versus OVA-SC 2 group and $^{\#\#\#\#}p < 0.0001$ versus OVA-IM 2 group on week 8, $^{*}p < 0.05$ versus OVA-SC 2 group and $^{\#\#\#\#}p < 0.0001$ versus OVA-IM 2 group on week 10, $^{****}p < 0.0001$ versus OVA-SC 2 group and $^{\#\#\#\#}p < 0.0001$ versus OVA-IM 2 group on week 12, $^{****}p < 0.0001$ versus OVA-SC 2 group and $^{\#\#\#\#}p < 0.0001$ versus OVA-IM 2 group on week 14.

patch, ensuring that the penetration and detachment of MNs do not rely solely on users correctly applying compression and shear force.

4. Conclusion

In this study, we developed a self-healing porous microneedle (PMN) patch via cryogenic micromoulding and phase separation for efficient loading and sustained delivery of diverse therapeutics. Compared to existing sustained-release drug delivery systems, the self-healing PMN patch offers several advantages. Firstly, due to its porous structure and self-healing ability, the PMNs patch allows for a post-loading approach that features a simple process, mild conditions, and the absence of harsh conditions (such as high temperature, organic solvents, and mechanical stirring), resulting in significantly improved stability for loaded drugs. The loading content of desired drugs can be controlled by adjusting the initial concentration of the incubation solution. Secondly, unlike conventional sustained-release systems or formulations that rely on the injection or surgical implantation, the administration of drug-loaded healed PMN patch simply requires the penetration of MNs into the skin with thumb press and detachment of MNs from the based substrate with a shear, resulting in a painless, user-friendly, and minimally invasive procedure. Last but not least, the PMNs are made of FDA-approved material (PLGA) with rational and ingenious design instead of newly synthesized materials, potentially facilitating their translation from bench to clinic. With further development and optimization, we anticipate that this microneedle technology may eventually help reduce the need for frequent administrations of drugs and vaccines, thereby improving patient compliance. Moreover, the proposed fabrication strategy holds promise for widespread use in developing a variety of porous materials for diverse applications, such as biosensors, tissue engineering, energy storage, and so on.

5. Experimental Section

Materials: PDMS was purchased from Dow Corning (USA). Poly(lactic-co-glycolic acid) (PLGA, Mw 45 kDa) was purchased from Daigang Biomaterial Co., Ltd. (China). Fluorescein isothiocyanate isomer I (FITC) was purchased from Macklin (China). Carbonate buffer (0.05 M, pH = 9.6), IgG, IgG1, IgG2a antibody, horseradish peroxidase (HRP)-conjugated goat anti-mouse IgG, IgG1, and IgG2a were purchased from Applygen (China). Optical cutting temperature (OCT) compounds were purchased from Sakura Finetek (Japan). 4% paraformaldehyde fix solution was purchased from Biosharp (China). 1,4-dioxane, phosphate buffered saline (PBS), and bovine serum albumin (BSA) sodium chloride were purchased from Sigma-Aldrich (USA). Ovalbumin (from chicken egg white, OVA) was purchased from Aladdin (China). DMEM, RPMI-1640, fetal bovine serum (FBS), 10 000 U mL^{-1} penicillin–streptomycin (P/S) were purchased from Thermo Fisher Scientific (USA). GOT/AST assay kit was purchased from Solarbio (China). Hematoxylin and eosin were purchased from Sigma-Aldrich (USA). Tween-20, TMB solution for ELISA, stop solution for TMB Substrate, LDH cytotoxicity assay kit, cell counting kit-8 (CCK-8) were purchased from Beyotime (China). Mouse ELISA kit of IFN-γ were purchased from Neo-Bioscience (China).

Cell Culture: The B16 melanoma cell line transfected with ovalbumin (B16-OVA) cells was purchased by the Meisen CTCC. B16-OVA cells were cultivated in DMEM that prepared with 10% fetal bovine serum (FBS) and 1% penicillin/streptomycin (P/S) in a culture dish at 37 °C in a humidified 5% CO_2 incubator. For subsequent cell tests, culture dishes with 80 – 90% confluence were utilized and the culture media was changed every two or three days.

Fabrication of Self-Healing PMN Patches: The pre-designed stainless steel MN templates served as the master mould. To create the negative mould of MNs, the master mould was replicated using a 10:1 ratio of PDMS (polydimethylsiloxane), with each needle cavity measuring 450 µm in diameter and 1200 µm in height. These needle cavities were arranged in a 10 × 10 array with a tip-to-tip spacing of 900 µm. A PLGA solution consisting of 1 mL 1,4-dioxane supplemented with 400 mg of PLGA was poured into the PDMS mould. The mould was then centrifuged at 3000 rpm for 3 min to ensure that the solution completely filled the needle cavities. Next, 180 µL of resin solution was cast into the substrate of the mould and exposed to UV light (365 nm, 100 mW cm^{-2}) for 30 s to solidify. After being frozen at −40 °C for 4 h and cryogenically demolded, a preformed MN patch was obtained. The resulting MN patch was immersed in deionized water to facilitate phase separation. Since 1,4-diaxane is miscible with water, PMNs can be soaked with a large amount of water repeatedly, and subsequently dried by freeze-drying to deplete the solvent. The final PMN patch was obtained after complete drying and transferred to a desiccator for storage until it is ready for use. For inducing the self-healing of PMNs, the PMN patch was exposed to mild infrared light (IR) for various durations (20, 40, 60, 80, and 100 min).

Morphology of Self-Healing PMN Patches: The MNs after cryogenic-demoulding, PMNs and healed PMNs were imaged by an invert fluorescence microscope (CKX53, Olympus) and a digital camera. The temperature of healing behavior of the PMNs was monitored by the infrared thermal imager. To visualize the pores inside and surface of PMNs and the healed PMNs, the samples were coated with platinum in a sputter coating system (JEC-3000FC, JEOL, Japan) and then imaged under JSM-IT800 scanning electron microscope (SEM, JEOL, Japan).

Mechanical Properties of Self-Healing PMN Patches: The mechanical properties of the PMNs and healed PMNs under different irradiation times of IR were measured using a displacement-force test station (Instron 68SC-05, USA). Briefly, an array patch of PMN and healed PMNs for different irradiation times (20, 40, 60, 80, and 100 min) was attached to a flat-rigid stainless steel, and the test sensor probe approached the MNs at a slow speed of 0.008 mm s^{-1} in a vertical direction. The images of PMN after compression test were photographed by an inverted fluorescence microscope (CKX53, Olympus). To assess the shear force of the healed PMNs patch after an irradiation time of 80 min, the patch was attached to a horizontally positioned rigid platform, with the microneedles facing sideways. The test sensor was positioned 1 mm away from the first row of healed PMNs and pressed vertically against the substrate at a low speed of 0.008 mm s^{-1}, covering the entire patch until reaching the end of the last row.

Skin Penetration of Self-Healing PMN Patches: Healed PMNs patch loaded with fluorescein isothiocyanate labelled ovalbumin (FITC-OVA) was inserted into the fresh porcine skin by finger press for 30 s. The microneedles were gently separated from the substrate by sliding along the surface of the porcine skin using a gentle shear force. After penetration, the porcine skin containing MNs and the separated substrate were imaged by an invert microscope (CKX53, Olympus). The porcine skin was further fixed with 4% paraformaldehyde and cut into 5 µm slices by a cryostat microtome (NX70, Thermo Scientific). The bright-field and fluorescence-field images of the slices were examined under an invert fluorescence microscope stereo microscope (SZX16, Olympus).

Drug Loading Capacity of Self-Healing PMN Patches: Fluorescein (376 Da), FITC-OVA (45 kDa), and fluorescein isothiocyanate-labelled dextran (FITC-Dex, 150 kDa) were chosen as model drugs with varying molecular weights. They were subsequently dissolved in phosphate-buffered saline (PBS, pH 7.4) at different concentrations (2, 5, 10, 15, and 20 mg mL^{-1}) to create the incubation solution. First, the mass of PMNs was recorded as v_0. Then, the mass of the PMNs after immersed in the incubation solution mentioned above for 10 min was recorded as v_1. Meanwhile, remove excess solution from the surface of the microneedle with

filter paper. Subsequently, the drug loading of PMNs was calculated using the following formula:

$$m = (v_1 - v_0) * c \quad (1)$$

where m is the drug loading capacity, v_0 is the mass of the PMNs, v_1 is the mass of PMNs after drug loading, and c is the concentration of the incubation drug solution. The bright and fluorescent fields of PMNs, as well as healed PMNs, were observed using an inverted fluorescence microscope (SZX16, Olympus). Furthermore, the stability of OVA-loaded MNs was detected before and after mild irradiation with infrared (IR) for 80 min. This was done using a BCA protein colorimetric assay kit and examined using a microplate reader (TECAN, Spark).

Drug Release and Degradation of Self-Healing PMN Patches In Vitro: Specifically, healed PMNs loaded with OVA and FITC-OVA were separated from the supporting substrate and then incubated in PBS at 37 °C. At predetermined time intervals, 20 µL of the release medium was collected and replaced with an equal amount of fresh PBS. The collected release media were quantitatively analyzed using a BCA protein colorimetric assay kit and examined with a microplate reader (TECAN, Spark). Simultaneously, the FITC-OVA-loaded healed PMNs after different incubation times were observed under an inverted fluorescence microscope (SZX16, Olympus). To assess the release profile of MTX, the collected release media were quantitatively analyzed using UV-visible spectroscopy to measure their absorbance at 302 nm.

In Vivo Drug Release of Self-Healing PMN Patches: The in vivo sustained release kinetic behavior of healed PMNs was studied on C57BL/6 mice (female, 8 weeks). The study was approved by the Animal Research Ethics Committee of Hangzhou Institute of Medicine (HIM), Chinese Academy of Sciences. The mice were dehaired under anaesthesia before use. FITC-OVA-loaded healed PMNs were vertically pressed into the mice's skin using a thumb for 30 s, followed by the application of shear force with a finger to remove the substrate. At predetermined time points (0, 10, 20, 30, 40, and 50 days), the mice were anesthetized and imaged using an in vivo imaging system (IVIS, PerkinElmer). Fluorescence images were collected using 480/520 nm excitation/emission filters, and the fluorescence intensity of the images was processed and analyzed using Living Image.

In Vivo Treatment of Psoriasis with Self-Healing PMN Patches: The study was approved by the Animal Research Ethics Committee of Hangzhou Institute of Medicine (HIM), Chinese Academy of Sciences (2023R0010). Imiquimod (IMQ)-induced psoriasis mouse model was established. Briefly, the BALB/c mice (male, 8–10 weeks) were dehaired under anaesthesia and 62.5 mg of IMQ cream was applied on the shaved skin of the mice. Meanwhile, the mice were randomly divided into eight groups and received different treatments for consecutive 7 days: control group (health mice without psoriasis), model group (psoriasis mice without treatment), MTX-oral×1 group (psoriasis mice with oral administration of MTX one time), MTX-oral×3 group (psoriasis mice with oral administration of MTX three times), MTX-topical×1 group (psoriasis mice with topical administration of MTX one time), MTX-topical×3 group (psoriasis mice with topical administration of MTX three times), blank healed PMNs group (psoriasis mice treated with blank healed PMNs) and MTX-healed PMNs×1 group (psoriasis mice treated with MTX-loaded healed PMNs one time). Due to the molecular weight of MTX (454 Da) falling between that of the carrier model drug fluorescein (376 Da) and OVA (45 kDa), the loading of MTX in PMNs can be achieved by immersing it in the incubation solution for 10 min, which is the same as the loading of fluorescein or OVA. For the mice in the treatment groups, a single administration dosage was 30 µg. Skin was imaged and body weight was monitored. During the treatment, the Psoriasis Area and Severity Index (PASI) score was recorded by grading erythema, scaling, and induration as 0 (no symptoms), 1 (mild), 2 (moderate), 3 (severe), or 4 (very severe). The skin thickness was measured daily for 7 days using a vernier caliper. After a 7-day treatment period, the mice were sacrificed, and their skin, liver, and spleen tissues were collected. The size of the spleen was documented through photography and weight measurement. Additionally, the activity of Glutamic Oxaloacetic Transaminase (GOT) in the liver was assessed using a GOT/AST kit to evaluate liver damage. The skin tissue was fixed with 4% paraformaldehyde and then sectioned for histological evaluation using H&E (hematoxylin & eosin) staining.

In Vivo Immunization of Antigen using Self-Healing PMN Patches: The study was approved by the Animal Research Ethics Committee of Hangzhou Institute of Medicine (HIM), Chinese Academy of Sciences (2023R0008; 2023R0009). In this study, OVA was used as model antigen. C57BL/6 mice (female, 8 weeks) were randomly distributed into five groups: untreated, blank healed PMNs, OVA-SC (subcutaneous injection of 80 µg OVA), OVA-IM (intramuscular injection of 80 µg OVA), and OVA-healed PMNs (healed PMNs loaded with 80 µg of OVA). Each group of mice only received one-time vaccination on day 0. The blood was collected to determine the level of anti-OVA IgG, IgG1 and IgG2a antibodies in serum on day 0, 10, 20, and 30. All the mice were sacrificed on day 30 and the major organs (heart, liver, spleen, lung, and kidney) were harvested for the following study.

A splenocyte proliferation and cytotoxic T lymphocyte (CTL) assay were performed. A single-cell suspension of splenocytes (5×10^5 per well) was plated in a 96-well plate with 50 µg mL^{-1} OVA and incubated at 37°C. The proliferation of splenocytes was measured using CCK-8 at 0 h and 72 h. The production of IFN-γ in the culture supernatants, after 72 h of incubation, was measured using a mouse IFN-γ ELISA kit. The CTL assay was conducted according to the manufacturer's protocol, using the CyQUANT LDH cytotoxicity kit. In brief, effector cells (splenocytes) and target cells (B16 melanoma cell line transfected with ovalbumin, B16-OVA) were co-cultured in U-bottomed 96-well plates at cell number ratios of 10:1, 50:1, and 100:1. After incubating for 2 h at 37°C, the lysed target cells were quantified. To analyze any organ damage following the vaccination process, the major organs were cryosectioned and stained with H&E.

Moreover, the long-term immunity elicited by different vaccination protocols was studied. BALB/c mice (male, 8 weeks) were randomly distributed into five groups

OVA-SC 1 group (subcutaneous injection of 80 µg OVA one time), OVA-SC 2 group ((subcutaneous injection of 80 µg OVA two times), OVA-IM 1 group (intramuscular injection of 80 µg OVA one time), OVA-IM 2 group (intramuscular injection of 80 µg OVA two time), and OVA-healed PMNs 1 group (one-time vaccination using the healed PMNs loaded with 80 µg of OVA). The first and second immunizations were conducted at week 0 and week 4, respectively. Blood samples were collected at predetermined time points to measure the levels of anti-OVA IgG, IgG1, and IgG2a in the serum using ELISA assay.

Statistical Analysis: All experiments used biological replicates that consisted of cells in non-repeated, independent cell culture wells or tissue samples from different animals, unless specified otherwise. Quantitative data are represented as mean ± s.d. Statistical analysis was performed by using two-tailed Student's *t*-test or original one-way ANOVA. $p < 0.05$ were considered statistically significant ($^{*}p < 0.05$, $^{**}p < 0.01$, $^{***}p < 0.001$, $^{****}p < 0.0001$). GraphPad Prism 8.3 was used for data analysis. Excel 2019 was used for calculating exact p value when $p < 0.0001$.

Supporting Information

Supporting Information is available from the Wiley Online Library or from the author.

Acknowledgements

H.C. acknowledges the financial support from the National Natural Science Foundation of China (No. 82202329), startup funding (No. 2021QD08-1; 2021QD08-2) supported by the Hangzhou Institute of Medicine, Chinese Academy of Sciences, and a research grant from Medcraft Biotech. Inc. (No. 2022HX01). The authors acknowledge the use of instruments at the Shared Instrumentation Core Facility at the Hangzhou Institute of Medicine, Chinese Academy of Sciences.

Conflict of Interest

Z.X.L. and H.C. are inventors of a patent that has been applied based on the data in this manuscript. H.C. is the scientific founder of a company that develops microneedles. The rest of the authors have no conflict of interest in this work.

Data Availability Statement

The data that support the findings of this study are available from the corresponding author upon reasonable request.

Keywords

cryogenic micromoulding, long-acting therapies, microneedles, self-healing, sustained release

Received: August 31, 2023
Revised: November 5, 2023
Published online:

[1] a) W. Li, J. Tang, D. Lee, T. R. Tice, S. P. Schwendeman, M. R. Prausnitz, *Nat. Rev. Mater.* **2022**, *7*, 406; b) S. Wang, R. Liu, Y. Fu, W. J. Kao, *Expert Opin Drug Deliv* **2020**, *17*, 1289.

[2] a) G. A. Roth, V. C. T. M. Picece, B. S. Ou, W. Luo, B. Pulendran, E. A. Appel, *Nat. Rev. Mater.* **2022**, *7*, 174; b) B. S. Ou, O. M. Saouaf, J. Baillet, E. A. Appel, *Adv Drug Deliv Rev* **2022**, *187*, 114401.

[3] a) K. M. Cirelli, D. G. Carnathan, B. Nogal, J. T. Martin, O. L. Rodriguez, A. A. Upadhyay, C. A. Enemuo, E. H. Gebru, Y. Choe, F. Viviano, C. Nakao, M. G. Pauthner, S. Reiss, C. A. Cottrell, M. L. Smith, R. Bastidas, W. Gibson, A. N. Wolabaugh, M. B. Melo, B. Cossette, V. Kumar, N. B. Patel, T. Tokatlian, S. Menis, D. W. Kulp, D. R. Burton, B. Murrell, W. R. Schief, S. E. Bosinger, A. B. Ward, et al., *Cell* **2019**, *177*, 1153; b) X. Wen, K. Xi, Y. Tang, J. Bian, Y. Qin, W. Xiao, T. Pan, X. Cheng, Z. Ge, W. Cui, *Small* **2023**, *19*, e2207030; c) T. Thambi, Y. Li, D. S. Lee, *J Control Release* **2017**, *267*, 57; d) Z. Li, W. Ho, X. Bai, F. Li, Y.-J. Chen, X.-Q. Zhang, X. Xu, *J Control Release* **2020**, *322*, 622.

[4] a) F. P. Pons-Faudoa, A. Ballerini, J. Sakamoto, A. Grattoni, *Biomed. Microdevices* **2019**, *21*, 47; b) J. W. Lee, J.-H. Park, M. R. Prausnitz, *Biomaterials* **2008**, *29*, 2113.

[5] H. Chang, M. Zheng, S. W. T. Chew, C. Xu, *Adv. Mater. Technol.* **2020**, *5*, 1900552.

[6] T. Sheng, B. Luo, W. Zhang, X. Ge, J. Yu, Y. Zhang, Z. Gu, *Adv Drug Deliv Rev* **2021**, *179*, 113919.

[7] A. H. Sabri, Y. Kim, M. Marlow, D. J. Scurr, J. Segal, A. K. Banga, L. Kagan, J. B. Lee, *Adv Drug Deliv Rev* **2020**, *153*, 195.

[8] a) Z. Chen, J. He, J. Qi, Q. Zhu, W. Wu, Y. Lu, *Drug Discov Today* **2020**, *25*, 1462; b) L. K. Vora, K. Moffatt, I. A. Tekko, A. J. Paredes, F. Volpe-Zanutto, D. Mishra, K. Peng, R. Raj Singh Thakur, R. F. Donnelly, *Eur. J. Pharm. Biopharm.* **2021**, *159*, 44.

[9] a) W. Li, R. N. Terry, J. Tang, M. R. Feng, S. P. Schwendeman, M. R. Prausnitz, *Nat. Biomed. Eng.* **2019**, *3*, 220; b) Y. Huang, H. Li, T. Hu, J. Li, C. K. Yiu, J. Zhou, J. Li, X. Huang, K. Yao, X. Qiu, Y. Zhou, D. Li, B. Zhang, R. Shi, Y. Liu, T. H. Wong, M. Wu, H. Jia, Z. Gao, Z. Zhang, J. He, M. Zheng, E. Song, L. Wang, C. Xu, X. Yu, *Nano Lett.* **2022**, *22*, 5944; c) Z. Yao, T. Xue, C. Cai, J. Li, M. Lu, X. Liu, T. Jin, F. Wu, S. Liu, C. Fan, *Adv Therap* **2020**, *3*, 2000025.

[10] a) J. V. Natarajan, C. Nugraha, X. W. Ng, S. Venkatraman, *J Control Release* **2014**, *193*, 122; b) M. Ye, S. Kim, K. Park, *J Control Release* **2010**, *146*, 241; c) S. Ahadian, J. A. Finbloom, M. Mofidfar, S. E. Diltemiz, F. Nasrollahi, E. Davoodi, V. Hosseini, I. Mylonaki, S. Sangabathuni, H. Montazerian, K. Fetah, R. Nasiri, M. R. Dokmeci, M. M. Stevens, T. A. Desai, A. Khademhosseini, *Adv Drug Deliv Rev* **2020**, *157*, 37.

[11] a) S. Y. Choi, S. J. Park, W. J. Kim, J. E. Yang, H. Lee, J. Shin, S. Y. Lee, *Nat. Biotechnol.* **2016**, *34*, 435; b) W. Jiang, R. Gupta, M. Deshpande, S. Schwendeman, *Adv Drug Deliv Rev* **2005**, *57*, 391.

[12] G. Liu, K. McEnnis, *Polymers* **2022**, *14*, 993.

[13] S. E. Reinhold, K.-G. H. Desai, L. Zhang, K. F. Olsen, S. P. Schwendeman, *Angew Chem Int Ed Engl* **2012**, *51*, 10800.

[14] H. Chang, S. W. T. Chew, M. Zheng, D. C. S. Lio, C. Wiraja, Y. Mei, X. Ning, M. Cui, A. Than, P. Shi, D. Wang, K. Pu, P. Chen, H. Liu, C. Xu, *Nat. Biomed. Eng.* **2021**, *5*, 1008.

[15] X. Sun, B. Xue, Y. Tian, S. Qin, L. Xie, *Appl. Surf. Sci.* **2018**, *462*, 633.

[16] C. C. Striemer, T. R. Gaborski, J. L. Mcgrath, P. M. Fauchet, *Nature* **2007**, *445*, 749.

[17] X. Lu, L. Miao, W. Gao, Z. Chen, K. J. Mchugh, Y. Sun, Z. Tochka, S. Tomasic, K. Sadtler, A. Hyacinthe, Y. Huang, T. Graf, Q. Hu, M. Sarmadi, R. Langer, D. G. Anderson, A. Jaklenec, *Sci. Transl. Med.* **2020**, *12*, eaaz6606.

[18] Y. Stetsyshyn, J. Raczkowska, O. Lishchynskyi, K. Awsiuk, J. Zemla, P. Dabczynski, A. Kostruba, K. Harhay, H. Ohar, B. Orzechowska, Y. Panchenko, P. Vankevych, A. Budkowski, *J. Mater. Chem. B* **2018**, *6*, 1613.

[19] M. R. Prausnitz, *Adv. Drug Delivery Rev.* **2004**, *56*, 581.

[20] S. Bao, B. Silverstein, *Ergonomics* **2005**, *48*, 288.

[21] E. Abd, S. A. Yousef, M. N. Pastore, K. Telaprolu, Y. H. Mohammed, S. Namjoshi, J. E. Grice, M. S. Roberts, *Clin Pharmacol* **2016**, *8*, 163.

[22] D. Peak, T. C. Werner, R. M. Dennin, J. K. Baird, *J. Chem. Phys.* **1983**, *79*, 3328.

[23] a) X. Xie, Y. Hu, T. Ye, Y. Chen, L. Zhou, F. Li, X. Xi, S. Wang, Y. He, X. Gao, W. Wei, G. Ma, Y. Li, *Nat. Biomed. Eng.* **2021**, *5*, 414; b) X. Xi, T. Ye, S. Wang, X. Na, J. Wang, S. Qing, X. Gao, C. Wang, F. Li, W. Wei, G. Ma, *Sci. Adv.* **2020**, *6*, eaay7735.

[24] H. C. Kim, Y. H. Choi, W. Bu, M. Meron, B. Lin, Y.-Y. Won, *Phys. Chem. Chem. Phys.* **2017**, *19*, 10663.

[25] M. Kemme, I. Prokesch, R. Heinzel-Wieland, *Polym. Test.* **2011**, *30*, 743.

[26] a) T. H. Baryakova, B. H. Pogostin, R. Langer, K. J. McHugh, *Nat. Rev. Drug. Discov.* **2023**, *22*, 387; b) J. Gao, J. M. Karp, R. Langer, N. Joshi, *Chem. Mater.* **2023**, *35*, 359.

[27] L. Xi, Z. Lin, F. Qiu, S. Chen, P. Li, X. Chen, Z. Wang, Y. Zheng, *Acta Pharm. Sin. B* **2022**, *12*, 339.

[28] C. Chaiyabutr, P. Punnakitikashem, N. Silpa-Archa, C. Wongpraparut, L. Chularojanamontri, *Clin Cosmet Investig Dermatol* **2022**, *15*, 2253.

[29] Q. Li, W. Liu, S. Gao, Y. Mao, Y. Xin, *BMC Immunol.* **2021**, *22*, 11.

[30] a) H. Shinno-Hashimoto, A. Eguchi, A. Sakamoto, X. Wan, Y. Hashimoto, Y. Fujita, C. Mori, M. Hatano, H. Matsue, K. Hashimoto, *Sci. Rep.* **2022**, *12*, 14738; b) L. Van Der Fits, S. Mourits, J. S. A. Voerman, M. Kant, L. Boon, J. D. Laman, F. Cornelissen, A.-M. Mus, E. Florencia, E. P. Prens, E. Lubberts, *J. Immunol.* **2009**, *182*, 5836.

[31] K. T. M. Tran, T. D. Gavitt, N. J. Farrell, E. J. Curry, A. B. Mara, A. Patel, L. Brown, S. Kilpatrick, R. Piotrowska, N. Mishra, S. M. Szczepanek, T. D. Nguyen, *Nat. Biomed. Eng.* **2021**, *5*, 998.

[32] F. Belardelli, *APMIS* **1995**, *103*, 161.
[33] a) H. Li, Z. Wang, E. A. Ogunnaike, Q. Wu, G. Chen, Q. Hu, T. Ci, Z. Chen, J. Wang, D. Wen, H. Du, J. Jiang, J. Sun, X. Zhang, G. Dotti, Z. Gu, *Natl Sci Rev* **2022**, *9*, nwab172; b) P. Liu, H. Du, Y. Chen, H. Wang, J. Mao, L. Zhang, J. Tao, J. Zhu, *J. Mater. Chem. B* **2020**, *8*, 2032; c) Y. T. He, L. Liang, Z. Q. Zhao, L. F. Hu, W. M. Fei, B. Z. Chen, Y. Cui, X. D. Guo, *J Drug Deliv Sci Tec* **2022**, *74*, 103518.
[34] a) H. Lee, G. Bonfante, Y. Sasaki, N. Takama, T. Minami, B. Kim, *Med Devices Sens* **2020**, *3*, e10109; b) G. Gao, L. Zhang, Z. Li, S. Ma, F. Ma, *ACS Biomater. Sci. Eng.* **2023**, *9*, 85.
[35] H. Abe, Y. Matsui, N. Kimura, M. Nishizawa, *Macromol. Mater. Eng.* **2021**, *306*, 2100171.
[36] M. Ochi, B. Wan, Q. Bao, D. J. Burgess, *Int. J. Pharm.* **2021**, *599*, 120450.
[37] W. Li, S. Li, X. Fan, M. R. Prausnitz, *J Control Release* **2021**, *339*, 350.